Available online at www.sciencedirect.com
ScienceDirect
Remote Sensing of Environment 107 (2007) 12–21
Remote Sensing of Environment
www.elsevier.com/locate/rse

Analysis of MODIS–MISR calibration differences using surface albedo around AERONET sites and cloud reflectance

A. Lyapustin [a,*], Y. Wang [a], R. Kahn [b], J. Xiong [c], A. Ignatov [d], R. Wolfe [c], A. Wu [e], B. Holben [c], C. Bruegge [b]

[a] University of Maryland, Baltimore County, and NASA Goddard Space Flight Center, mail code 614.4, Greenbelt, MD 20771, United States
[b] NASA Jet Propulsion Laboratory, Pasadena, CA 91109, United States
[c] NASA Goddard Space Flight Center, Greenbelt, MD 20771, United States
[d] NOAA/NESDIS, Camp Springs, MD 2074, United States
[e] Science Systems and Applications, Inc., Lanham, MD 20706, United States

Received 17 March 2006; received in revised form 26 September 2006; accepted 30 September 2006

Abstract

MODIS and MISR are two Earth Observing System instruments flown onboard the Terra satellite. Their synergistic use could greatly benefit the broad user community by ensuring a global view of the Earth with high-quality products. A necessary condition for data fusion is radiometric calibration agreement between the two instruments. Earlier studies showed about 3% absolute radiometric difference between MISR and respective MODIS *land* bands in the visible and near-IR spectrum, which are also used in aerosol and cloud research. This study compared two surface albedo products derived from MODIS and MISR L1B data using the AERONET-based Surface Reflectance Validation Network (ASRVN). The ASRVN shows a positive MISR–MODIS albedo bias of +(0.01–0.03). Cross-sensor calibration inconsistencies were identified as a primary cause of the albedo biases. To establish an independent MODIS–MISR calibration link, top-of-atmosphere MODIS and MISR reflectances were regressed against each other over liquid water clouds. The empirical regression results have been adjusted for the differences in the respective MISR and MODIS spectral responses using radiative transfer simulations. The MISR–MODIS band gain differences for the top-of-atmosphere reflectance estimated with this technique are +6.0% in the Blue, +3.3% in the Green, +2.7% in the Red, and +0.8% in the NIR band. Applying the derived values to rescale the MODIS or MISR L1B data is shown to significantly reduce the cross-sensor ASRVN surface albedo biases. An absolute calibration scale for both sensors could be established based on independent ground-based measurements of the surface albedo at selected AERONET sites.

Keywords: MODIS; MISR; Calibration; AERONET; Surface albedo; Cloud regression

1. Introduction

MODIS and MISR are two major Earth Observing System (EOS) (NASA, 1999) instruments flown onboard of TERRA satellite, and used to produce global information about aerosol, cloud and land surface parameters. Each instrument has advantages, such as the large number of spectral bands and daily global coverage of MODIS, and the unique multi-view-angle capabilities of MISR. An optimal synergy of MODIS–MISR products could greatly benefit the broad user community by ensuring consistent, high-quality products providing a global view of Earth's land, ocean and atmosphere.

At present, the absolute radiometric scales of MISR spectral bands and respective MODIS *land* bands are known to differ by about 3% over most of the visible spectrum (Bruegge et al., 2004; Thome et al., 2004; Xiong et al., 2005b). The two instruments employ different calibration strategies, and the differences of about 3% are within the uncertainties of the respective calibration methods. A brief overview of the MODIS and MISR calibration procedures and associated accuracies is given in Section 2.

* Corresponding author.
E-mail address: Alexei.l.Lyapustin.1@gsfc.nasa.gov (A. Lyapustin).

0034-4257/$ - see front matter © 2006 Elsevier Inc. All rights reserved.
doi:10.1016/j.rse.2006.09.028

The goal of this work is to characterize the difference in the MODIS–MISR relative calibration using the AERONET-based Surface Reflectance Validation Network (ASRVN). The ASRVN [*in preparation*] is an operational processing system that receives MODIS and MISR calibrated top-of-atmosphere (TOA) reflectance (L1B) data around AERosol RObotic NETwork (AERONET) (Holben et al., 1998) sites globally, and uses AERONET well-calibrated aerosol and water vapor data to independently and self-consistently derive surface bi-directional reflectance factor (BRF) and albedo. The ASRVN retrievals show a systematic positive MISR–MODIS bias of +(0.01–0.03). Because spectral band differences are accounted for through the radiative transfer, the most likely explanation for the bias is a calibration inconsistency between the sensors. The ASRVN is briefly introduced in Section 3, and albedo comparison is described in Section 4.

To independently assess the MISR–MODIS calibration differences, a new ASRVN function was developed for this study. It regresses MISR–MODIS TOA reflectances over liquid water clouds, with a theoretical correction for the sensors spectral differences. The methodology and results of the regression analysis are described in Section 5. This section also investigates the effect of different solar irradiance models used in MODIS and MISR calibration that affects radiances and fluxes in the Blue band. Section 6 demonstrates that normalizing MODIS or MISR reflectances to a common radiometric scale using the adjustment factors derived in Section 5 significantly reduces the surface albedo biases in all bands. Finally, Section 7 summarizes and concludes this study.

The structure of this paper reflects evolution of our research from perspective of the multi-sensor data user for the land discipline applications, emphasizing the importance of a consistent calibration. It also shows how comparison of the ASRVN surface albedo, derived from different sensors with AERONET ancillary data and reduced uncertainties, may guide the multi-sensor calibration analysis. Similar approaches based on the use of derived products to detect and quantify sensor calibration uncertainties, have been previously explored in the ocean and atmospheric applications using the water leaving radiance and aerosol optical depth products, respectively (Evans & Gordon, 1994; Ignatov, 2002; Kahn et al., 2005). These approaches emphasize user's perspective to the sensor calibration and articulate the fact that an ultimate measure of the calibration is quality and consistency of the derived products, in contrast with the classical calibration approaches which attempt to characterize and reconcile satellite TOA reflectances or radiances. Furthermore, radiances or reflectances are not easy to compare from different sensors or platforms, which might have different spectral response functions (such as e.g. Terra MISR and MODIS in this study), different overpass times or different sun-view geometry (e.g. Terra MODIS versus Aqua MODIS). On the other hand, these problems can be addressed using the derived geophysical products. Studies linking multi-sensor products and calibration are expected to become more common in the near future, and will be eventually considered a part of the global calibration and validation system as the remote sensing community gears towards the Global Earth Observation System of Systems era.

2. Overview of MODIS and MISR calibration in the reflective solar bands

The two sensors employ different calibration strategies: MODIS uses onboard calibration devices whereas MISR relies on a combination of vicarious calibration experiments and on-board band-to-band and camera-to-camera relative calibration tests, to establish its absolute radiometric scale. Both MODIS and MISR teams have been conducting comprehensive calibration and characterization instrument analyses (Bruegge et al., 2004, 2002; Chrien et al., 2002; Diner et al., 2004; Kahn et al., 2005; Xiong et al., 2005a,b, 2003c,b, 2005c, 2003a,d). The two instruments have shown a good agreement for lunar observations taken early on in the TERRA satellite mission (Bruegge et al., 2004). The systematic discrepancy in absolute radiance was found later in the vicarious experiments over both bright desert targets (Diner et al., 2004) and ocean, in low light conditions (Kahn et al., 2005).

2.1. MODIS

MODIS makes observations in 20 reflective solar bands (RSB) at three nadir spatial resolutions (250 m for bands 1–2, 500 m for bands 3–7, and 1 km for bands 8–20) over a wide field-of-regard (±55°). MODIS L1B geolocated and radiometrically calibrated data products include TOA reflectance factors and spectral radiances. In order to monitor and maintain on-orbit calibration accuracy and data product quality, the instrument was designed with a set of on-board calibrators, including a solar diffuser (SD) and a solar diffuser stability monitor (SDSM) system for the RSB calibration, and a spectro-radiometric calibration assembly for the sensor's spectral and spatial characterization (Guenther et al., 2002; Xiong et al., 2005a,b, 2003c,b,a). The RSB calibration accuracy requirements (1σ at the typical scene radiances) are ±2% for the reflectance, and ±5% for the radiance product. MODIS RSB calibration uses look-up tables derived from SD/SDSM measurements. On-orbit, the SD/SDSM system is operated on a bi-weekly basis (weekly in first year) to track the RSB response changes.

MODIS SD panel is made of space grade Spectralon material, with a near-Lambertian reflectance profile in the RSB spectral range. Its bi-directional reflectance factor (BRF) was carefully characterized pre-launch by the instrument vendor (Raytheon/Santa Barbara Remote Sensing) using a comparison approach with reference samples traceable to the reflectance standards of the National Institute of Standards and Technology (NIST). The BRF profiles for some reflective solar bands were also validated on-orbit using data collected during spacecraft maneuvers (Xiong et al., 2003d). Solar exposure of the SD panel causes the SD BRF to degrade. The rate of SD BRF changes is wavelength dependent. For this reason, the SDSM is operated during each scheduled SD calibration event. The SDSM, which has its own spectrally-filtered detectors, works as a ratioing radiometer. It tracks the SD BRF on-orbit degradation using its simultaneous responses to the direct sunlight and that diffusely reflected from the SD panel (Xiong et al., 2003c). For Terra MODIS, the response changes have been approximately 2% at 0.47 μm (band 3) and less than 1% at 0.86 μm (band 2) per year over its nearly

6 years of on-orbit operation. Numerous L1B look-up tables have been updated to capture these changes and to maintain the calibration and data product quality. Details of the history of L1B code and look-up table updates can be found from MODIS Characterization Support Team web page (http://www.mcst.ssai.biz/mcstweb/index.html).

2.2. MISR

Data from both vicarious calibration experiments and the on-board calibration system play key roles in the MISR radiometric calibration process (Bruegge et al., 2004, 2002). Vicarious field data provide input to a radiative transfer code that simulates MISR band-weighted top-of-atmosphere radiances. The MISR calibration process is adjusted so the Level 1B2 Geolocated Radiance Product values equal those measured during the 2000 field campaign at Lunar Lake, Nevada. Subsequent vicarious calibration experiments have served to verify the accuracy of the radiance data product. Annual field measurements are made at homogeneous desert playa sites such as Lunar Lake, Railroad Valley, Ivanpah, and Black Rock Desert, all in Nevada, under clear sky and low aerosol conditions, to verify the results and help monitor calibration changes. The precision of the vicarious absolute calibration is estimated to be 2–4% (1σ), and is best for the MISR Green and Red bands, whereas the band-to-band and camera-to-camera uncertainties appear to be in the 1–2% range (Bruegge et al., 2004).

MISR response degradation has been approximately 2% per year over the first five years in flight. To account for drifts from the 2000 scale determination, the MISR team makes use of an on-board calibrator. Here bi-monthly observations are made of sunlight reflected by diffuse-reflecting, Lambertian standards. These panels are made of pristine Spectralon, and have not degraded during the first five years of the mission (e.g., Chrien et al., 2002). On-board photodiode detectors measure the panel-reflected radiances. Differences between the camera and diode fields-of-view and spectral responses are taken into account as part of the calibration analysis, and the panels themselves are assumed white, based on pre-launch studies. The individual cameras and secondary diodes then view the sun-lit panels simultaneously to complete the camera-to-camera on-board calibration. Since the cameras do not all view the panels at the same angle as the calibration diodes, panel bi-directional reflectance functions are used. These were also measured pre-launch, and are checked periodically by another on-board diode package mounted on a goniometer. The detectors were initially calibrated using the 2000 vicarious calibration campaign observations. Degradation of the photodiodes is accounted for by response adjustments against a specific photodiode, the Blue High-Quantum-Efficiency diode, which has been stable throughout the mission to date (Chrien et al., 2002).

To further validate the band-to-band and camera-to-camera radiance scales, the MISR Team analyzed a set of observations taken when the Terra spacecraft was rotated to observe the moon, multiple observations over uniform, dark water having identical geometry relative to the solar equator, and radiance comparisons with MODIS (Bruegge et al., 2004; Diner et al., 2004). The low-light-level calibration was tested further by assessing MISR radiances relative to a radiative transfer model constrained by AERONET observations taken around deep ocean island sites (Kahn et al., 2005). To first order, MISR reported absolute radiances are 3% higher than MODIS, when compared over homogenous scenes. This has been traced to differences between the vicarious calibration scale adopted for MISR, and the on-board standard used for MODIS.

3. AERONET-based surface reflectance validation network

The ASRVN was originally designed as a validation tool for the moderate resolution (~1 km) global surface reflectance products from the EOS sensors. It is implemented as a dedicated workstation with a set of coordinated data-reception protocols and processing algorithms. The ASRVN receives operational MODIS and MISR L1B (geolocated and calibrated) data from Goddard and Langley Distributed Active Archive Centers (DAAC), respectively, subsetted into 32×32 km^2 areas around more than 160 AERONET sites worldwide. Upon receiving AERONET water vapor and aerosol information, the ASRVN performs an automatic atmospheric correction deriving the BRF, albedo, top-of-canopy vegetation index, and radiative fluxes for each instrument independently.

The ASRVN atmospheric correction algorithms for MISR and MODIS data are based on the semi-analytical Green's function solution (Lyapustin & Knyazikhin, 2001, 2002) that allows accurate and numerically efficient retrievals. Our radiative transfer algorithm calculates the in-band reflectances for specific sensor band-pass functions with an accuracy of several tenths of a percent (Lyapustin, 2003). The ASRVN atmospheric correction algorithm for MISR is documented in Lyapustin et al. (2006). It takes advantage of near-simultaneous multi-angle reflectances measured by MISR. The input MISR L1B2T (terrain-corrected) data have a constant resolution of 1.1 km for all view angles (from 0 to 70.5°). The ASRVN algorithm for MODIS was developed recently and will be described in detail elsewhere. Here, we only outline its main features.

Because MODIS provides a single-angle measurement at a time at any given location, the processing algorithm first accumulates several days of TOA measurements from different orbits corresponding to different solar-view angles. To mitigate the effect of view zenith angle (VZA)-dependent pixel size, MODIS measurements are first re-projected and gridded that effectively reduces its at-nadir resolution by a factor of 2. Then, the algorithm simultaneously inverts multi-angle gridded TOA radiance for three parameters of the Li Sparse–Ross Thick (LSRT) BRF model (Lucht et al., 2000), assuming stable surface conditions. This assumption is tested with a threshold-based change detection algorithm, similar to (Roy et al., 2002). The ASRVN atmospheric correction is applied to both cloud-free and cloudy satellite data. Cloud screening is performed afterwards based on the "history" of surface albedo for a given pixel. The thresholds were empirically derived to allow only relatively continuous and gradual temporal changes in the spectral surface albedo. Using temporal consistency has proven to be superior to the operational cloud masks used currently, that rely solely on instantaneous sensor measurement.

The reliance on a unified and validated radiative transfer model and use of common BRF models ensures consistency of the ASRVN surface albedo products derived from different sensors, provided their TOA reflectances are consistent.

4. ASRVN albedo comparison

For each instrument, the ASRVN products are stored in both swath and gridded format. The gridded products are used for cross-sensor comparisons and time series analysis.

Fig. 1 shows the ASRVN surface albedo from MISR and from MODIS for two AERONET sites, Mongu, Zambia, and Goddard Space Flight Center, USA. For mapping purposes, the MODIS data are reprojected and gridded to the MISR spatial resolution of 1.1 km. The spatial pattern and surface contrast are well reproduced from both sensors. However, at both sites and in all bands, the MISR albedo tends to be systematically higher than its MODIS counterpart. A similar bias is observed at other AERONET locations. On average, the magnitude of bias is +0.014±0.014 in the Blue, +0.011±0.007 in the Green, +0.022±0.015 in the Red, and +0.008±0.010 in the NIR bands. More accurate estimates of the cross-sensor albedo biases are deferred until more representative ASRVN MODIS statistics are accumulated. The regular subsetting of MODIS data over AERONET sites started only in November of 2005 and so far we have found only 15 cloud-free or partially clear cases for which comparisons with MISR can be made. In contrast, albedo and BRF from MISR L1B reprocessed collection 4 data are available for two periods from 2000–2001 and from 2005–2006.

Several sources of uncertainties may affect comparisons between the ASRVN albedos from different sensors. One is related to spectral variability of reflectance of different land cover types. Several examples of soil and vegetation reflectance from the USGS spectral library (Clark et al., 2003) are shown in Fig. 2. This variability can be partially responsible for the difference in the Red band, and for a smaller fraction of difference in the Blue band, because the band-passes and effective band center wavelengths are different. However, it cannot explain the systematic bias in the Green and NIR bands where the spectral response functions (Fig. 2) are close.

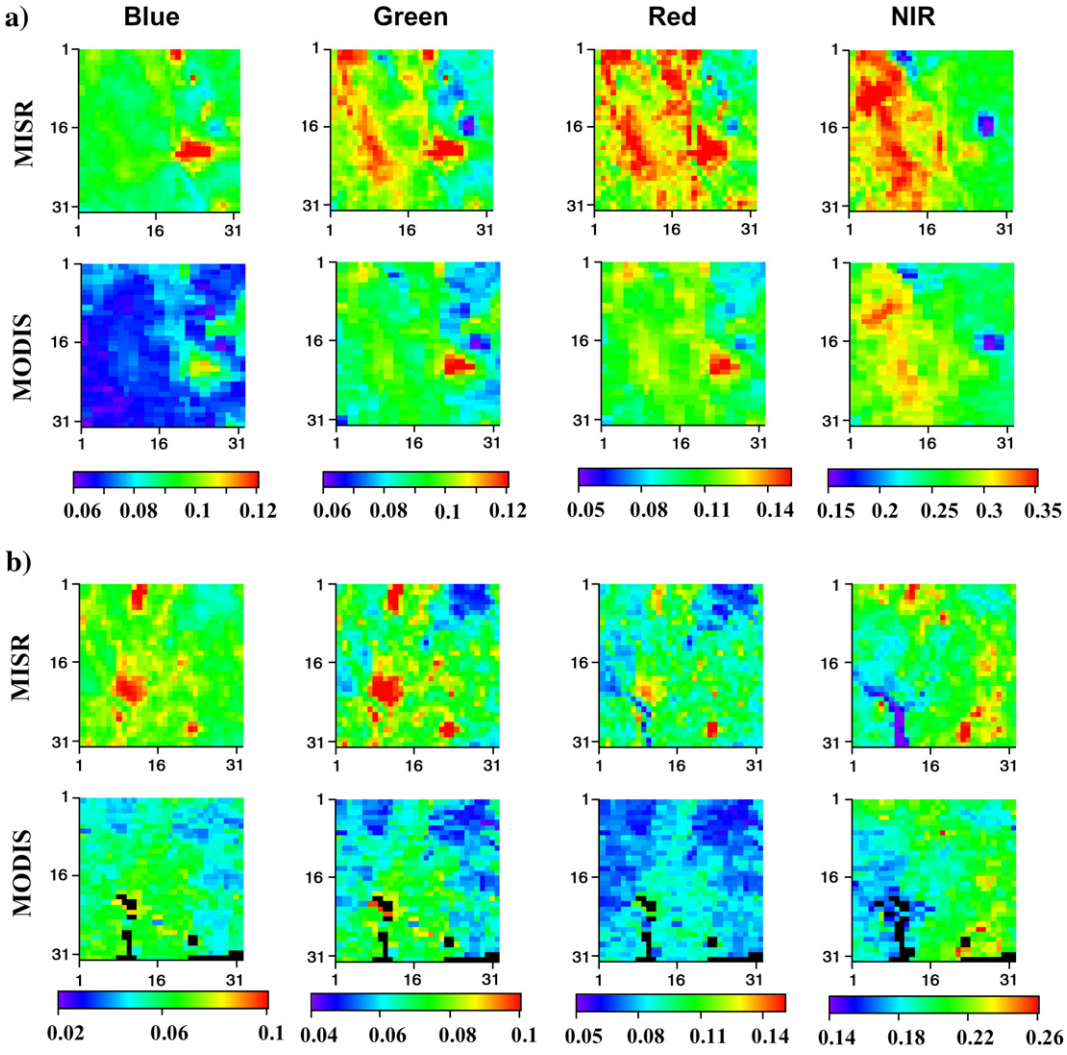

Fig. 1. Comparison of MISR and MODIS surface albedo retrieved for AERONET sites at a) Mongu, July 13, 2005, and b) GSFC, February 21, 2006. Black color in MODIS data shows areas with no retrievals due to cloud contamination.

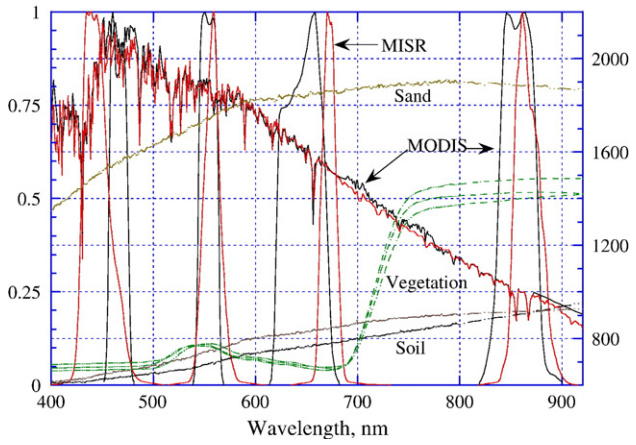

Fig. 2. Relative spectral response functions of MISR (red) and MODIS land channels (black). Also shown are models of MODIS and MISR spectral solar irradiance ($\frac{W}{m^2\,\mu m}$), and reflectance spectra of several types of soil, sand, and vegetation. (For interpretation of the references to color in this figure legend, the reader is referred to the web version of this article.)

Another source of uncertainty is associated with the differences in the MODIS and MISR view geometries. The BRF is derived in the restricted domain of view angles and extrapolated to the full hemisphere with the LSRT model in order to calculate the albedo. The derived LSRT model allows us to fit the TOA reflectance quite well, usually to within several percent of either MISR or MODIS measurements. However, if the actual BRF of the surface deviates from the LSRT model assumed in the retrievals, extrapolation of the BRF outside of the domain of observations will involve some errors. Generally, albedo is better constrained by the MISR view geometry which has a larger VZA range (±70.5°). To quantify this source of error, we compared MISR albedo retrieved using 9, 7, and 5 view angles. In the last two cases, the highest VZAs have been cut off symmetrically. The albedo derived using 7 angles (±60°) matched well the 9-angle values with the difference of ±0.001. With 5 view angles (±45.6°), more representative of the MODIS VZAs, the change was still less than ±0.003, which can be regarded as the uncertainty due to view geometry. Another potential source of uncertainty, the difference in azimuthal angle, cannot be assessed from experimental data alone because MISR measurements do not provide azimuthal coverage. It is known from model-based analysis, though, that the effect of azimuthal angle is less important (Jin et al., 2002).

Uncertainty in the AERONET ancillary information is another source of error in this approach. Typical AOT uncertainty for a field sunphotometer is 0.01–0.02 and is spectrally dependent. The aerosol microphysical properties and concentration are retrieved to within several percent ($RMSE_{sky} \leq 1$–3%) from the best-fit residual to the almucantar sky radiances (Dubovik et al., 2000). Errors in AERONET data may affect MISR and MODIS albedos differently, because the MISR albedo is based on near-simultaneous measurements, whereas the MODIS albedo is a result of 4–16 consecutive days of observations. Yet, these errors are expected to be distributed randomly and therefore should not contribute to the systematic bias.

Analysis in this section indicates that a positive MISR–MODIS surface albedo bias is present in all four bands, despite the large uncertainties due to the insufficient MODIS statistics. These uncertainties will be reduced in the future as more ASRVN retrievals from MODIS are accumulated. Quick assessment of different sources of this bias suggests that cross-sensor inconsistencies in the respective L1B reflectances are the most plausible cause.

5. MISR–MODIS cross-calibration over clouds

To mitigate the ASRVN albedo biases observed in Section 3, an independent cross-calibration analysis was performed using optically thick water clouds. Such clouds are spectrally flat in the visible and NIR region and thus can serve as a calibration transfer standard as described in Section 5.1. This approach has been used to cross-calibrate the AVHRR sensors (Doelling et al., 2004; Vermote & Kaufman, 1995).

The interpretation of the empirical regression slopes in terms of the sensors calibration gain ratios is not straightforward because of the spectral differences between the MISR and MODIS bands. This effect is small for spectrally close bands, but it is important and must be considered at the level of accuracy aimed at in this study (e.g. Heidinger et al., 2002). To quantify this effect, radiative transfer model (RTM) simulations were performed (Section 5.2). The empirical regression results were then adjusted for the MISR–MODIS spectral differences, to facilitate their interpretation in terms of sensors gain ratio.

5.1. Empirical results

For this work, the ASRVN was augmented to include a separate processing of MISR TOA reflectances from the nadir camera (An, VZA <15°) and corresponding MODIS near-nadir reflectances. MODIS and MISR data are first re-projected and then averaged over an area of 32×32 km^2 to minimize the effect of different projections and pixel sizes. The MISR L1B2T data were multiplied by cosine of the solar zenith angle for consistency with MODIS L1B TOA reflectance (given by Eq. (2), Section 5.2). The experimental regressions are shown in Fig. 3, top row. These data represent most of the AERONET stations on different continents, covering different seasons, and the full range of solar zenith angles. Fig. 3 has $N=1500$ data points accumulated between November 2005 and February 2006.

The regression only contains points for which the ASRVN cloud mask algorithm detected at least 50% cloudy pixels inside the averaging box (32×32 km^2). With this definition, regression points may include a mixture of clear pixels, and continuous or broken clouds of different optical depths, which can be both liquid water and ice. We have tested the sensitivity of the empirical regression to the 50% threshold varying it from 40% to 70% and found that it has very little effect on the regression parameters. For example, adding non-cloudy pixels in the averaging box only slightly increases scatter around the low end of regression in the visible bands and practically has no effect on its slope and offset. The effect of scatter is larger

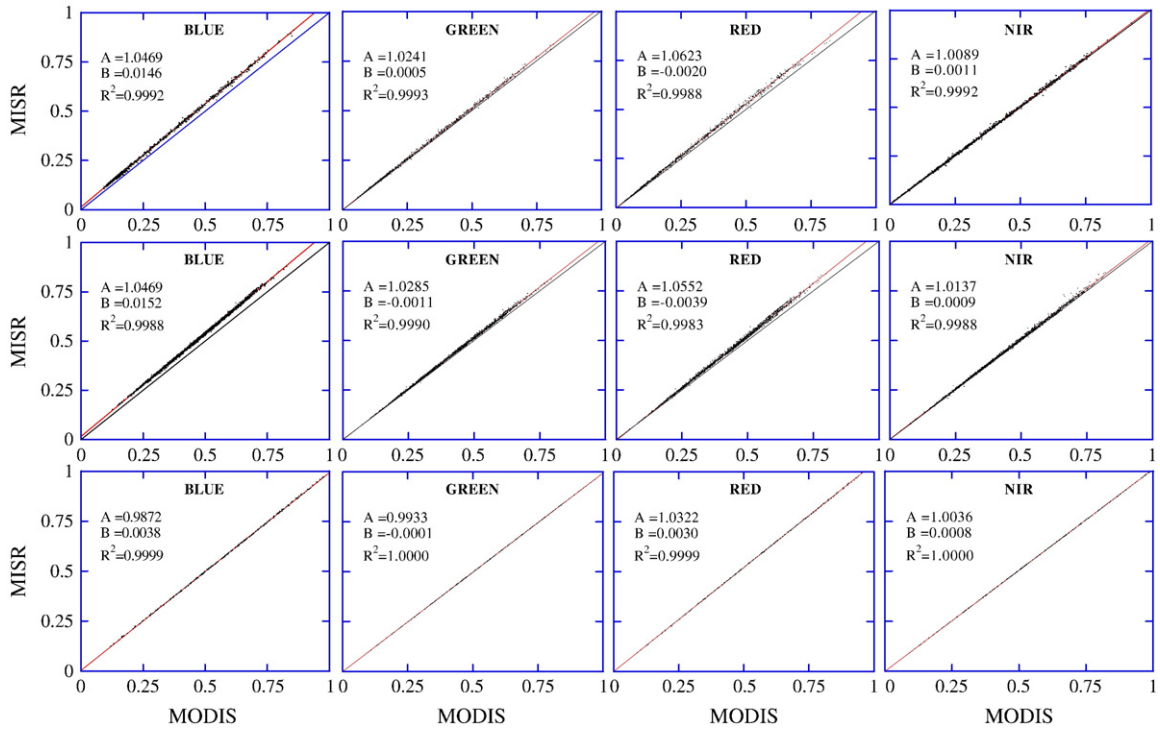

Fig. 3. Experimental and theoretical regressions of MODIS–MISR TOA L1B reflectance over clouds. The plots of top and middle rows represent data collected over the land and over the ocean. The bottom row shows theoretically calculated regression lines.

in the NIR band, but still the effect on the regression parameters was minimal. By trial and error, the 50% threshold was found to be adequate.

As a sensitivity check, and for better agreement with our theoretical analysis (see Section 5.2), an independent set of MODIS and MISR L1B data was collected over the ocean in pristine maritime conditions: off the southern coast of Peru, coasts of California, Namibia and Zimbabwe, and off the coast of south-east Asia, 44 MODIS and corresponding MISR granules in total. The MODIS Cloud Phase (MOD06) product was used to select points representing liquid water clouds. The view geometry was restricted to the non-glint conditions defined as $R_{CM}<0.02$, where R_{CM} is a calculated Cox and Munk (1954) reflectance of the roughened water surface at the wind speed of 10 m/s. This restriction helped us to eliminate a few remaining outliers in the data. The regressions for $N=1600$ points collected in January–February 2006 are shown in Fig. 3, middle row.

Interestingly, the results for the carefully screened oceanic water clouds are very close to the mixed-case results obtained over land. This may indicate that ice clouds can also be used as targets for the cross-calibration analysis using this method. The regression results over the land and over the ocean are practically identical in the Blue band. In the other three bands, the differences in the slopes and intercepts are larger, but they are still statistically insignificant (i.e. less than uncertainties of the regression coefficients).

The regressions obtained represent different regions of both the Northern and Southern hemispheres. The regression lines were found to stabilize after about $N=500$ data points have been accumulated. Nevertheless, larger and more representative statistics continue to be collected, to investigate possible regional and seasonal variability in experimental regressions.

The empirical regression coefficients $\mathrm{MISR}=A\times\mathrm{MODIS}+B$ from Fig. 3 are summarized in Table 1. Here, the "Measured" row lists the average coefficients between the land and the ocean. Except for the Blue band, the offset of the regression is within the regression error and should be set to zero. This is expected because the radiometric offsets in both MISR and MODIS reflectance are specified from space counts and are therefore known very accurately. The reason for the offset anomaly in the Blue band is unknown and is being investigated further. The average empirical slopes are 1.047, 1.026, 1.059 and 1.011 for the Blue, Green, Red and NIR bands, respectively. In the next subsection, theoretical simulations are performed and used to adjust these empirical estimates for the MISR–MODIS spectral differences.

5.2. Simulations

Liquid water clouds have been simulated using Mie theory and a narrow-band radiative transfer code that can account for

Table 1
Summary of slope and offset regression coefficients

	A_B	B_B	A_G	B_G	A_R	B_R	A_{NIR}	B_{NIR}
1. Measured	1.047	0.015	1.026	−0.003	1.059	−0.003	1.011	0.001
2. Simulated	0.987	0.004	0.993	−0.000	1.032	0.003	1.003	0.001
3. Difference	0.060	0.011	0.033	−0.003	0.027	−0.006	0.008	0.000

The "Measured" coefficients represent the average between the land and the ocean. The numbers have been rounded to third significant digit.

the difference in the relative spectral responses (RSR) of the sensors analyzed. The simulated spectral TOA radiance is expressed as:

$$L_{\Delta\lambda} = \int \frac{F_\lambda}{\pi} I_\lambda h_\lambda \mathrm{d}\lambda \Big/ \int h_\lambda \mathrm{d}\lambda, \quad (1)$$

where F_λ is the extraterrestrial spectral solar irradiance, I_λ is monochromatic TOA radiance calculated for $F_\lambda = \pi$, h_λ is RSR of sensor. The TOA radiance and reflectance (R) are related via the band-dependent solar irradiance ($F_{\Delta\lambda}$),

$$L_{\Delta\lambda} = RE_{\Delta\lambda}/\pi, \quad E_{\Delta\lambda} = \int F_\lambda h_\lambda \mathrm{d}\lambda \Big/ \int h_\lambda \mathrm{d}\lambda. \quad (2)$$

The standard MODIS L1B reflectance product is corrected for out-of-band spectral contributions, whereas the MISR L1B reflectance is not (this correction is made later during L2 processing). To take this difference into account, the spectral limits of integration were selected to represent the in-band spectral intervals for MODIS, and the total spectral interval where RSR is defined (365–1100 nm) for MISR (Bruegge et al., 1999).

The radiative transfer calculations in this work were done using the SHARM code (Lyapustin, 2005) and the Interpolation and Profile Correction (IPC) method (Lyapustin, 2003). The IPC method is designed for fast line-by-line calculations in the spectral interval of interest with flexible spectral resolution of 0.01–1 cm^{-1} and an accuracy of several tenths of a percent. The line-by-line calculations are then integrated directly with solar irradiance and sensor' band-pass functions. The RTM included absorption of 7 major atmospheric gases (H_2O, CO_2, O_3, CH_4, NO_2, CO, N_2O) calculated for the HITRAN-2000 (Rothman et al., 2003) database using a Voigt vertical profile, and the Atmospheric Environmental Research continuum absorption model (Mlawer et al., in preparation). For radiative transfer in clouds, the SHARM code uses the Delta-M method.

To study the possibility of using both cloudy and clear-sky conditions for the calibration analysis, the RTM used different surfaces types with high-resolution reflectance spectra taken from the USGS (Clark et al., 2003) and ASTER (http://speclib.jpl.nasa.gov) spectral libraries. Our analysis for clear-sky conditions showed that the calculated slope and offset have a very weak dependence on aerosol type and concentration which can be neglected for the purpose of this work. On the other hand, they do depend on the solar zenith angle and show considerable variability over different land cover types. Similar results are known from experimental Landsat cross-calibration studies (Teillet et al., in press). For these reasons, further analysis will be limited to cloudy conditions.

The radiative transfer calculations were done with constant cloud top height (2 km) and column water vapor (1.5 cm) with the US 1976 Standard Atmosphere profile. The water clouds were modeled using a log-normal size distribution with mean radius r_g=6, 10, 15, 20 μm, and standard deviation σ_g=0.1, 0.35, scalable cloud optical depth τ_c=3.7–130, and optical spectral properties of water from Hale and Querry (1973). The mean radius for the log-normal distribution is close to the effective radius, typically used in cloud research and defined as a ratio of the third and the second moments of the size distribution. For example, for the simulated cases with σ_g=0.1, 0.35, the ratio of radii is r_g/r_{eff}=1.025 and 1.28, respectively.

A sensitivity study of theoretical regression coefficients shows that natural variability of cloud droplet size, cloud top height, and atmospheric moisture play relatively minor roles, causing a factor of 4–10 smaller variation than the band gain differences studied (see Appendix A). The calculated theoretical regressions are shown in the bottom row of Fig. 3. They are linear in the full dynamic range of the signal with non-linearity less than 0.5%, and have very little scatter. The theoretical slopes are 0.987, 0.993, 1.032, and 1.004 in the Blue, Green, Red and NIR bands, respectively.

In the future, we may extend the RTM to include ice clouds, to better represent a mixture of the real ASRVN conditions. The ice clouds may be as good a target as water clouds for our analysis because of the large size of scattering ice crystals and absence of absorption features in the visible-NIR spectral range. However, modeling ice cloud is complicated by a large diversity of ice particle shapes and models of scattering.

5.3. Spectral adjustment of the empirical regression. Solar irradiance model

To interpret the slopes of the empirical regression in terms of gain ratios, the numbers in the 1st row of Table 1 must be corrected using the theoretically expected slopes in the 2nd row. Results of this correction are listed in the 3rd row. With this adjustment, MISR–MODIS band gain differences for TOA reflectance become +6.0%, +3.3%, +2.7%, and +0.8% for the Blue, Green, Red and NIR bands, respectively. The only band with a non-zero intercept is the Blue. More analyses are needed to fully understand the anomalous behavior of this band.

MODIS TOA reflectance is a primary L1B product obtained by normalizing the detector's readout with the SD measurement. The L1B radiance is calculated from the reflectance using the in-band irradiance which depends on the selected spectral solar irradiance model (SIM). The MISR primary validated L1B product is absolute radiance. The MISR calibration coefficients were adjusted in the vicarious calibration experiments by fitting the measured TOA radiance to the radiance calculated with selected SIM. The L1B reflectance is calculated from TOA radiance by dividing by the SIM-dependent total spectral irradiance. Thus, the L1B MODIS and MISR reflectance does not depend on SIM, whereas spectral irradiance and L1B radiances (fluxes), as well as the calibration coefficients in case of MISR depend on the chosen solar irradiance model.

Presently, due to the lack of high accuracy exo-atmospheric measurements, the SIM is not standardized. The models used by the MODIS and MISR calibration teams are slightly different (see Fig. 2). MODIS uses a combination of Thuillier et al. (1998) (0.4–0.8 μm), Neckel and Labs (1984) (0.8–1.1 μm), and Smith and Gottlieb (1974) (above 1.1 μm), whereas MISR uses the values of solar irradiance published by the World Climate Research Program (Wehrli, 1985). The maximal difference for the spectral intervals covered by the band-pass

Table 2
Ratio of in-band irradiance calculated with MODIS and MISR solar irradiance models ($E_{\Delta\lambda}^{\mathrm{MODIS\_SIM}}/E_{\Delta\lambda}^{\mathrm{MISR\_SIM}}$) in MISR and MODIS land channels

Sensor/band	Blue	Green	Red	NIR
MODIS	1.0361	1.0040	0.9984	1.0029
MISR	1.0212	1.0028	1.0010	1.0067

functions is in the blue part of spectrum. Our radiative transfer model uses a high-resolution (1 cm^{-1}) theoretical model of Kurucz (1997).

We calculated spectral irradiance $E_{\Delta\lambda}$ (Eq. (2)) using both MODIS and MISR SIMs. The ratio of these values is given in Table 2 for MODIS bands and MISR spectral channels. Not unexpectedly, the difference in SIMs significantly affects the Blue band whereas in the other bands the effect is small. Thus, the difference in the solar irradiance model results in 2.1% to 3.6% of the radiance difference in the Blue band.

The above values of spectral irradiance were also compared with $E_{\Delta\lambda}$ computed with the high-resolution Kurucz solar model. In the Blue–Red bands, it agreed well with results obtained with MISR SIM, and in the Green-NIR bands it agreed with results obtained with MODIS SIM. On the other hand, slope and offset of the theoretically calculated regressions practically do not depend on SIM.

6. Effect of gain adjustment on the surface albedo comparisons

In the next step, the derived gain adjustment factors (6.0%, 3.3%, 2.7% and 0.8%) were applied to the L1B reflectance of one of the sensors followed by ASRVN re-processing. The cross-sensor albedo agreement clearly improved in all bands. Summarizing the improvement for all matching cases, the average bias reduced from +0.014, +0.011, +0.022, +0.008 to +0.002, +0.006, +0.015, +0.005 in the Blue, Green, Red, and NIR bands, respectively. The remaining albedo difference between MISR and MODIS is still relatively high in the Red band, but this may be caused by factors other than calibration. Because the centers and band-passes of MODIS and MISR red bands are quite different, it is not possible to differentiate between the effects of calibration and of spectral surface variability (Fig. 2) without detailed knowledge of the surface reflectance spectra.

7. Conclusions

This work started with the observation of the systematic biases between the surface albedo and BRF retrieved by ASRVN from MODIS and MISR data near AERONET sites, which is most likely explained by calibration inconsistencies between the two sensors. To verify this observation, an independent cross-calibration analysis was performed using TOA regression method over clouds.

The following cross-sensor calibration biases for L1B reflectance were found: 6.0% in the Blue, 3.3% in the Green, 2.7% in the Red, and 0.8% in the NIR bands. The difference in the MODIS–MISR solar irradiance models does not affect L1B reflectance, but it causes about 3% difference in the L1B radiance in the Blue band. These discrepancies are generally within the calibration uncertainties of the two instruments, 2–4% for MISR absolute radiance, and 2% for MODIS reflectance. However, they may lead to observable systematic differences in the geophysical parameters affecting multi-instrument data analysis and data fusion approaches. For example, the derived band gain difference is spectrally-dependent, increasing from NIR to Blue band. This can be important e.g. for the aerosol particle size and mixture composition retrievals as it affects spectral slope of aerosol optical thickness (e.g. Ignatov, 2002). Furthermore, the systematic difference in surface albedo of 0.01–0.03 in the visible part of spectrum may bias retrievals of vegetation parameters, important for global carbon analysis.

Application of the derived gain correction factors made it possible to reduce cross-instrument albedo biases effectively by a factor of 2–3 in the Blue, Green and NIR bands, although it did not cancel the differences entirely. Albedo agreement in the Red band has also improved, and the remaining bias of 0.015 may be caused by factors other than calibration, as explained in Section 6.

Regressing TOA reflectances from MISR and MODIS against each other over dense liquid water clouds to check cross-sensor calibration consistency is a promising technique when applied to data from the same platform. However, its application to data from different orbits may be subject to time–space mismatch, affecting the correlation and limiting applicability of this method. On the other hand, the relative cross-calibration can be achieved through statistical matching of ASRVN albedo products from different sensors. This method can be applied to sensors from different orbits because it corrects for the difference in the view-illumination geometry (BRF effect). Work is underway to demonstrate this.

One way to adjust the absolute radiometric scales from different orbital instruments would be to provide continuously operating reliable ground-based albedo measurements in selected highly homogeneous locations with different levels of surface brightness, next to AERONET sites. The relative spectral albedo measurements are easier in that they do not pose such rigorous calibration requirements as the absolute radiance measurements. If such measurements were available, the ASRVN could provide mutually consistent absolute calibration factors for the reflectance scales for different instruments.

Acknowledgements

This work was supported by the NASA EOS Science (Dr. D. Wickland) and NPP (Dr. J. Gleason) grants. The first author would like to thank Dr. S. Platnick (NASA GSFC) for discussion on regression analysis over clouds, and Dr. D. Diner (NASA JPL) for general suggestions on the paper. The work of R. Kahn is supported in part by NASA's Climate and Radiation Research and Analysis Program, under H. Maring, and in part by the EOS-MISR instrument project; it is performed at the Jet Propulsion Laboratory, California Institute of Technology, under contract with NASA. The work of A. Ignatov was funded under the NASA EOS/CERES Project (NASA contract L-90987C).

Insightful comments from three anonymous reviewers were helpful to improve the presentation of this paper. The views, opinions, and findings contained in this report are those of the authors and should not be construed as an official NASA, NOAA or U.S. Government position, policy, or decision.

Appendix A. Sensitivity of theoretical regression to atmospheric variability

Extensive simulations were conducted for the near-nadir view geometry (VZA <15°) and a wide range of solar zenith angles (0° ≤ SZA ≤ 75°) studying the effect of cloud droplet size distribution, water vapor and cloud top height variations on the regression coefficients. Simulations revealed the following results:

- The effect of solar zenith angle is small in the Blue and Red bands, and it is negligible in the Green and NIR. On the other hand, the regression is slightly non-linear. For instance, increase of SZA range to 0°–75° from the range 0°–51° changes slope of regression from 0.989 to 987 in the Blue, and from 1.029 to 1.032 in the Red.
- Table A1 shows dependence of the regression coefficients on the effective size of water droplets. Blue and Red bands, in which the band-pass functions between MODIS and MISR differ most, were chosen for this sensitivity check. With the modal droplet radius changing from 6 to 20 μm, the slope of the regression changes from 0.993 to 0.978 in the Blue, and from 1.029 to 1.037 in the Red bands. The category "All" gives the average coefficients for the cumulative regression, which might be a little skewed towards clouds having the smallest effective radii. This happens because small droplets produce the highest optical depth in Mie calculations at the same droplet concentration. In turn, this gives the points with highest radiance, which may offset the total regression somewhat. In the future, we may weight our calculations for different radii with realistic regional cloud droplet size probability distribution functions, derived, for example, from the MODIS cloud product (MOD06).
- Table A2 shows that the regression slope in the Blue band is only weakly sensitive to the cloud top height. This sensitivity is due to the Rayleigh scattering above the cloud. In the Red band, this effect is about a factor of 2.5 smaller and is probably caused by the re-distribution of water vapor absorption above the cloud. There is practically no dependence in the spectrally close Green and NIR bands.
- The regression slope for the Red and NIR bands has a rather weak dependence on the column water vapor (Table A2), as long as the high moisture conditions (≈3.5–5 cm), typical of tropical geographical belt, are avoided.

Table A1
Dependence of slope in the Blue and Red bands on the effective droplet size

r_g, μm	6	10	15	20	All
A_B	0.991	0.986	0.980	0.976	0.987
A_R	1.029	1.035	1.036	1.037	1.032

Simulations were done for 1976 US Standard Atmospheric Profile, with the column atmospheric water vapor column of 1.5 cm and cloud top height of 2 km.

Table A2
Effect of cloud top height (H_c) and column water vapor (CWV) on the slope of regression, calculated for r_g=10 μm

	H_c (1–5 km)	CWV (0.4–2.0–5.0 cm)
A_B	0.984–0.991	–
A_G	–	–
A_R	1.034–1.037	1.033–1.037–1.052
A_{NIR}	–	1.002–1.008–1.017

The dependence on the cloud top height was calculated for CWV=0.5 cm. The dependence on the CWV was evaluated for H_c=2 km.

Thus, simulations show that sensitivity of this method to the natural atmospheric variability is relatively weak, about a factor of 4–10 smaller than the calibration difference effects we are studying. This makes clouds a good target for characterization of calibration difference between different instruments simultaneously observing the same cloud fields.

References

Bruegge, C. J., Abdou, W. A., Diner, D. J., Gaitley, B. J., Helmlinger, M. C., Kahn, R. A., et al. (2004). Validating the MISR radiometric scale for the ocean aerosol science communities. *Proceedings of the The International Workshop on Radiometric and Geometric Calibration, December 2–5, 2003, Gulfport, Mississippi* Rotterdam, Netherlands: A. A. Balkema Publishers.

Bruegge, C. J., Chrien, N. L., Ando, R. R., Diner, D. J., Helmlinger, M. C., Abdou, W. A., et al. (2002). Early validation of Multi-angle Imaging Spectro-Radiometer (MISR) radiometric scale. *IEEE Transactions on Geoscience and Remote Sensing*, *40*(7), 1500−1511.

Bruegge, C. J., Chrien, N. L., & Diner, D. J. (1999, December). *Level 1 in-flight radiometric calibration and characterization algorithm theoretical basis*.Jet Propulsion Laboratory, JPL D-13398, Rev. A. 128 pp.

Chrien, N. L., Bruegge, C. J., & Ando, R. R. (2002). Multi-angle Imaging SpectroRadiometer (MISR) On-Board Calibrator (OBC) In-flight Performance Studies. *IEEE Transactions on Geoscience and Remote Sensing*, *40*(7), 1493−1499.

Clark, R. N., Swayze, G. A., Wise, R., Livo, K. E., Hoefen, T. M., Kokaly, R. F., et al. (2003). *USGS Digital Spectral Library splib05a, USGS Open File Report 03-395.*

Cox, C., & Munk, W. (1954). Measurements of the roughness of the sea surface from photographs of the Sun's glitter. *Journal of the Optical Society of America*, *44*, 838−850.

Diner, D. J., Kahn, R. A., Bruegge, C. J., Martonchik, J. V., Abdou, W. A., Gaitley, B. J., et al. (2004). Refinements to MISR's radiometric calibration and implications for establishing a climate-quality aerosol observing system. *Proceedings of SPIE*, *5652*, 57−65.

Doelling, D., Nguyen, L., & Minnis, P. (2004). On the use of deep convective clouds to calibrate AVHRR data. *Proceedings of SPIE*, *5542*, 281−289.

Dubovik, O., Smirnov, A., Holben, B. N., King, M. D., Kaufman, Y. J., Eck, T. F., et al. (2000). Accuracy assessments of aerosol optical properties retrieved from AERONET sun and sky-radiance measurements. *Journal of Geophysical Research*, *105*, 9791−9806.

Evans, R. H., & Gordon, H. (1994). Coastal zone color scanner system calibration: A retrospective examination. *Journal of Geophysical Research*, *99*, 7293−7307.

Guenther, B., Xiong, X., Salomonson, V. V., Barnes, W. L., & Young, James (2002). On-Orbit performance of the Earth Observing System Moderate Resolution Imaging Spectroradiometer; first year of data. *Remote Sensing of Environment*, *83*, 16−30.

Hale, G. M., & Querry, M. R. (1973). Optical constants of water in the 200-nm to 200 μm wavelength region. *Applied Optics*, *12*, 555−563.

Heidinger, A. K., Cao, C., & Sullivan, J. (2002). Using MODIS to calibrate AVHRR reflectance channels. *Journal of Geophysical Research*, *107*, 4702. doi:10.1029/2001JD002035

Holben, B. N., Eck, T. F., Slutsker, I., Tanré, D., Buis, J. P., Setzer, A., et al. (1998). AERONET — A federated instrument network and data archive for aerosol characterization. *Remote Sensing of Environment*, *66*, 1−16.

Ignatov, A. (2002). Sensitivity and information content of aerosol retrievals from AVHRR: Radiometric factors. *Applied Optics*, *41*, 991−1011.

Jin, Y. F., Gao, F., Schaaf, C. B., Li, X. W., Strahler, A. H., Bruegge, C. J., et al. (2002). Improving MODIS surface BRDF/albedo retrieval with MISR multiangle observations. *IEEE Transactions on Geoscience and Remote Sensing*, *40*, 1593−1604.

Kahn, R., Li, W. -H., Martonchik, J., Bruegge, C., Diner, D., Gaitley, B., et al. (2005). MISR low-light-level calibration, and implications for aerosol retrieval over dark water. *Journal of the Atmospheric Sciences*, *62*, 1032−1062.

Kurucz, R. L. (1997). The solar irradiance by computation. (Available at). http://cfaku5.cfa.harvard.edu/papers/irradiance/

Lucht, W., Schaaf, C. B., & Strahler, A. H. (2000). An algorithm for the retrieval of albedo from space using semiempirical BRDF models. *IEEE Transactions on Geoscience and Remote Sensing*, *38*, 977−998.

Lyapustin, A. (2003). Interpolation and Profile Correction (IPC) method for shortwave radiative transfer in spectral intervals of gaseous absorption. *Journal of the Atmospheric Sciences*, *60*, 865−871.

Lyapustin, A. (2005). Radiative transfer code SHARM for atmospheric and terrestrial applications. *Applied Optics*, *44*, 7764−7772.

Lyapustin, A., & Knyazikhin, Yu. (2001). Green's function method in the radiative transfer problem. I: Homogeneous non-Lambertian surface. *Applied Optics*, *40*, 3495−3501.

Lyapustin, A., & Knyazikhin, Yu. (2002). Green's function method in the radiative transfer problem. II: Spatially heterogeneous anisotropic surface. *Applied Optics*, *41*, 5600−5606.

Lyapustin, A., Wang, Y., Martonchik, J., Privette, J., Holben, B., Slutsker, I., et al. (2006). Local analysis of MISR Surface BRF and albedo over GSFC and Mongu AERONET sites. *IEEE Transactions on Geoscience and Remote Sensing*, *44*, 1707−1718.

Mlawer, E. J., Tobin, D. C., & Clough, S. A. (in preparation). *A Revised Perspective on the Water Vapor Continuum: The MT_CKD Model*.

NASA (1999). In M. King, & R. Greenstone (Eds.), *EOS reference handbook: a guide to earth science enterprise and the earth observation system* (pp. 355). Greenbelt, MD: EOS Project Science Office, NASA/Goddard Space Flight Center.

Neckel, H., & Labs, D. (1984). The solar radiation between 3300 and 12500 A. *Solar Physics*, *90*, 205−258.

Rothman, L. S., Barbe, A., Benner, D. C., Brown, L. R., Camy-Peyret, C., Carleer, M. R., et al. (2003). The HITRAN Molecular Spectroscopic Database: Edition of 2000 Including Updates through 2001. *Journal of Quantitative Spectroscopy & Radiative Transfer*, *82*, 5−44.

Roy, D. P., Lewis, P. E., & Justice, C. O. (2002). Burned area mapping using multi-temporal moderate spatial resolution data — A bi-directional reflectance model-based expectation approach. *Remote Sensing of Environment*, *83*, 263−286.

Smith, E. V. P., & Gottlieb, D. M. (1974). Solar flux and its variations. *Space Science Reviews*, *16*, 771−802.

Teillet, P. M., Markham, B. L., & Irish, R. R. (in press). Landsat cross-calibration based on near simultaneous imaging of common ground targets. *Remote Sensing of Environment*.

Thome, K., Biggar, S., & Choi, H. J. (2004). Vicarious calibration of TERRA ASTER, MISR, and MODIS. *Conference on Earth Observing Systems IX, Aug. 2–6, 2004Earth Observing Systems*, *Vol. IX* (pp. 290–299).

Thuillier, G., Herse, M., Simon, P. C., Labs, D., Mandel, H., Gillotay, D., et al. (1998). The visible solar spectral irradiance from 350 to 850 nm as measured by the SOLSPEC spectrometer during the ATLAS I mission. *Solar Physics*, *177*, 41−61.

Vermote, E., & Kaufman, Y. (1995). Absolute calibration of AVHRR visible and near-IR channels using ocean and cloud views. *International Journal of Remote Sensing*, *16*(13), 2317−2340.

Wehrli, C. (1985). *Extraterrestrial solar spectrum. WRC PMOD Pub.*, *Vol. 615*.

Xiong, X., Che, N., & Barnes, W. (2005). Terra MODIS on-orbit spatial characterization and performance. *IEEE Transactions on Geoscience and Remote Sensing*, *43*, 355−365.

Xiong, X., Che, N., & Barnes, W. L. (2005). Five-year of Terra MODIS on-orbit spectral characterization. *Proceedings of SPIE — Earth Observing Systems X*, *5882*, 58820R. doi:10.1117/12.614090

Xiong, X., Chiang, K., Esposito, J., Gunther, B., & Barnes, W. L. (2003). MODIS on-orbit calibration and characterization. *Metrologia*, *40*, 89−92.

Xiong, X., Chiang, K., Guenther, B., & Barnes, W. L. (2003). MODIS thermal emissive bands calibration algorithm and on-orbit performance. *Proceedings of SPIE — Optical Remote Sensing of the Atmosphere and Clouds III*, *4891*, 392−401.

Xiong, X., Erives, H., Xiong, S., Xie, X., Esposite, J., Sun, J., et al. (2005). Performance of Terra MODIS solar diffuser and solar diffuser stability monitor. *Proceedings of SPIE — Earth Observing Systems X*, *Vol. 5882*, 58820S. doi:10.1117/12.615334

Xiong, X., Sun, J., Esposito, J., Guenther, B., & Barnes, W. L. (2003). MODIS reflective solar bands calibration algorithm and on-orbit performance. *Proceedings of SPIE — Optical Remote Sensing of the Atmosphere and Clouds III*, *4891*, 95−104.

Xiong, X., Sun, J., Esposito, J., Liu, X., Barnes, W. L., & Guenther, B. (2003). On-orbit characterization of a solar diffuser's bi-directional reflectance factor using spacecraft maneuvers. *Proceedings of SPIE — Earth Observing Systems VIII*, *5151*, 375−383.